AIAA JOURNAL
Vol. 34, No. 5, May 1996

Performance of a Hypersonic Twin-Nozzle System

Alfred E. Beylich*
Rheinisch Westfälischen Technischen Hochschule Aachen, 52056 Aachen, Germany

A numerical investigation of a planar twin-nozzle system is made on the basis of previous experimental and numerical studies that indicated that the performance of single expansion ramp nozzles, suitable for the propulsion of any type of hypersonic cruise vehicle, can possibly be improved by the application of a bypass jet and gas injection at the ramp. The assumption of planar flow is justified by the flow properties in the near-field of a jet issued from a large-aspect-ratio slit nozzle. Systematic variations of the stagnation state and the dimensions of the secondary nozzle are performed and indicate that a good control of the primary jet channel shaping—and therefore also of the pressure distribution along the ramp contour—can be achieved by using a cold secondary jet that then acts as a kind of gaseous wall. The mass flux of the secondary jet must be of the order of the primary jet flux to obtain a satisfactory shaping effect over a sufficiently large distance. For far off-design cases, however, overexpansion of the primary nozzle jet still will result in flow recompression by shock waves and flow separation in downstream regions of the ramp contour. It is shown that wall bleeding in small sections of the wall is one possibility to influence and to stabilize the thrust vector control.

Nomenclature

b = orifice slit width, cm
C_b = fraction of primary jet mass flux
c = sound speed, cm/s
c_0 = reference speed, cm/s
D_i = exit height of nozzle i, cm
E = sum of internal and kinetic energy, cm^2/s^2
$[\boldsymbol{F}, \boldsymbol{G}]$ = flux vector of $\boldsymbol{U}$, (g/cm^2s, g/cms^2, g/cms^2, g/cm^3)
H = total enthalpy, cm^2/s^2
H_a = altitude, km
h = orifice slit height, cm
L = length of ramp, cm
$\dot{m}_i$ = mass flux in nozzle i, g/(scm)
N_g = number of grid points
n, n_∞ = time step counter, total number of steps
p = static pressure, $g/(cms^2)$, bar
$\hat{Q}$ = limiter function in total variation diminishing scheme
$\boldsymbol{q}$ = heat flux vector, g/s^3
$R(x)$ = ramp contour, cm
R_g = gas constant, $cm^2/(s^2K)$
R_0 = primary nozzle throat height, scaling length, cm
Re_0 = Reynolds number, $\rho_a c_a R_0/\mu_a$
$\boldsymbol{S}$ = thrust vector/unit length, g/s^2, N/cm
T = temperature, K
t = independent variable, time, s
$\boldsymbol{U}$ = vector of conservative quantities, (g/cm^3, g/cm^2s, g/cm^2s, g/cms^2)
$\boldsymbol{u}$ = velocity vector, (u, v), cm/s
$\boldsymbol{W}_i$ = vector of state at location i, $(p_i, T_i, \boldsymbol{u}_i)$
$[x, y]$ = coordinates in physical space, cm
α_0 = shifting angle for primary nozzle
α_s = thrust vector angle
$\beta_{i,l/u}$ = lower/upper exit angle of nozzle i
γ = ratio of specific heat capacities, 1.4
$\Delta\rho$ = residual
$\Delta\rho_{\text{cell}}$ = residual per grid point, $\Delta\rho/N_g$
ϵ^* = scaling factor
$[\eta, \xi]$ = coordinates of mapped field
$\kappa_{x,y}$ = power law exponent for grid clustering, x, y direction
λ_t = thermal conductivity, $gcm/(s^3K)$
μ = dynamic viscosity, g/(cms)
ρ = density, g/cm^3
τ = stress tensor, $g/(cms^2)$
Π = pressure ratio, p_{10}/p_a
ω = exponent of viscosity temperature law, 0.62

Subscripts and Superscripts

a = outer flow
e = nozzle exit, end of cowl
i, j = grid points
n = Laval nozzle exit, time step
r = recompression point
w = wall
wi = locations at the ramp; for $i = 1 - 4$, $x_i = 8.3, 12.7, 17.5, 22.8$ cm
0 = stagnation state
1 = primary nozzle
2 = secondary nozzle
~ = nondimensionalized quantities

I. Introduction

THE idea to replace in space transportation systems the rocket propulsion by air-breathing devices during passage through the lower atmosphere leads to concepts of hypersonic cruise vehicles consisting of structures with airframe–integrated scramjet engines. In the case of a space plane, the first stage of such a system will be designed for altitudes up to $H_a = 35$ km and speeds corresponding to Mach numbers of $M_a = 6$–8. Once the decision is made to place the propulsion system underneath the airframe body, one of the major design problems consists in the requirement to adjust to the varying flight conditions for optimum performance. The most important influence comes from the change of the background pressure over two orders of magnitude during an ascent up to H_a. Therefore it is necessary to adjust the cross sections of the air intake and the propulsion nozzle according to the local flight conditions. For the simplest design concept, this leads to rectangular shapes for an air intake, with parts of the forebody acting as a supersonic precompression surface, and a nozzle with a part of the afterbody acting as a single expansion ramp nozzle (SERN).

Once this concept is accepted, one is faced with a considerable set of complex problems. It is evident that, for an optimization of the integrated system, the interdependence of the performance of the components can be properly treated only in an iterative procedure. But as a first step, it seems sensible to begin with studies of partial problems by using models for the components of the system, like the lifting body, the air intake, or the nozzle. Therefore, this study will be limited to problems of gasdynamics.

Received Jan. 21, 1995; revision received June 7, 1995; accepted for publication Jan. 2, 1996.

*Professor, Mechanical Engineering, Templergraben 55. Member AIAA.

The present work is concerned, as part of a concerted effort, with the performance of the nozzle jet, its interaction with the airframe, and with the outer flow. Previous experiments using a simple afterbody model and cold flow[1] had quickly revealed qualitatively that, for the design case, thrust vector control seems to be possible but also that the flowfield is complex and three dimensional. Problems arise for the lower altitude off-design cases because of overexpansion of the supersonic jet along the ramp. Experimenting with a bypass jet[2] and bleeding[3] indicated that some improvement of the performance is possible. Although such experiments are very valuable because of the quick information that they yield, it does not seem feasible to approach the problem further systematically by experiment alone because of the large number of parameters. Thus, a less expensive and faster numerical study may help to determine the sensitivity of various parameter variations to select optimized versions of nozzle systems.

The following reasoning leads us to abandon the previously used classification bypass jet and rather to speak of the primary and the secondary nozzle. We want to stress that the secondary jet is an important constitutive part of the total thrust vector system and not only used for primary jet shaping. Since mixing inside a real jet engine may not be achieved and will cause total pressure losses[4] and since, for example, boundary-layer scooping may create an additional mass flux that has to be used in some manner, it is justified to study a twin-nozzle system where the individual nozzles may have largely different stagnation conditions.

Models of SERN nozzles using cold flow[5,6] and high enthalpy flow[7] have been studied experimentally as well as numerically.[5,8] Recently, nozzle systems with an additional bypass nozzle[1] and an additional secondary nozzle were also studied numerically.[9] In the following, we shall approach the twin-nozzle concept by describing its evolution from the Laval nozzle. Then the design case will be studied, followed by an identification of some of the pertinent parameters of the system and the discussion of their influence on the flowfield and the performance of the nozzle, especially for off-design situations. Finally, the influence of gas bleeding from the ramp on thrust vector control will be studied for some cases of the far off-design state.

II. Design of the Twin-Nozzle Model System

With regard to possible later experiments, we shall study a system having the dimensions of a small model with the flow of a simple gas like air. For the stagnation conditions, fairly realistic values will be chosen. We develop the system by going through a series of characteristic steps that will lead to the idealized model system. Beginning with an ideal Laval nozzle (see Fig. 1), one will achieve optimal efficiency when at the exit the flow speed and the pressure are equal to the outer flow values, i.e., if $u_{1e} = u_a$ and $p_{1e} = p_a$. Now, when selecting either the stagnation state gas temperature T_{10} or the exit temperature T_{1e} one may obtain, from ideal isentropic relations, the stagnation conditions for the nozzle, W_{10}. The thrust can be obtained from the selection of the critical cross section of the nozzle where, for the planar case, we shall take the half-diameter R_0 as the characteristic length. It turns out that, for a full-scale hypersonic cruise vehicle, $R_0 \approx 50$ cm, and as a consequence of this, a full-scale Laval nozzle would be about 40–50 m long. Even with a cutoff, such a system could not be integrated into the airframe, because of the enormous drag and the large exit diameter of about 55 R_0 for the planar case. Therefore, in the next step (step 2) the lower part of the Laval nozzle below the symmetry line is removed and the lower nozzle wall is cut off almost up to the critical cross section. Since the flow acceleration is largest in the throat region and the Mach number increases rapidly here, a removal of the lower wall near $M_{1e} \approx 3$ is a good compromise. On the other hand, since a deviation from the optimum efficiency is small even when a large part of the downstream section of the nozzle is removed, a large part of the upper contour having a length L_{cut} will be cut off. Since $p_{1e} > p_a$, the removal of the lower guiding wall causes the gas flow to expand like a free jet into the lower region of the flowfield. As a result of this the thrust vector S is rotated towards a positive angle α_s. In addition, because of the removal (cutting or scarfing) of the side walls, there is a sidewise expansion on a different scale. This effect is well known from studies of jets issued from slit orifices.[10] The expansion in a plane

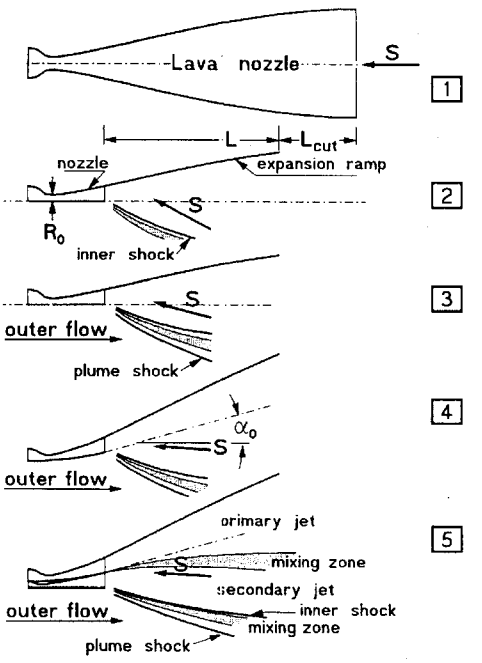

Fig. 1 Evolution steps of twin nozzle.

perpendicular to the slit, which scales with the slit height h, is rather rapid, whereas the expansion parallel to the slit scales with the slit width b and is slow. A supersonic cell of almost planar flow with an extension of the order of the slit length is created downstream of the nozzle exit. This behavior justifies, to a certain extent, the assumption of a planar flowfield near the nozzle. Many details of the cell structure of the SERN free jet can be explained using results from studies of jets from slit orifices. The overall planar jet cell structure scales with h and the pressure ratio $\Pi = p_{10}/p_a$, whereas the round orifice cell structure scales with orifice size and $\Pi^{1/2}$. In its details, the flow and the cell structure become very complex and are three dimensional in the downstream region. When exposing the nozzle jet to an outer hypersonic flow (step 3) with the state W_a (we shall neglect perturbations of this outer flow due to shocks, rarefaction waves, and boundary layers that would be caused by a forebody), the displacement by the jet creates a plume shock outside the mixing layer. The angle of this oblique plume shock surface changes with distance from the nozzle exit and is dependent on the outer state W_a, as well as on the local state in the jet at the nozzle exit. This interaction results in a reduction of the thrust vector angle α_s that, however, would still be too large for any practical application even considering the effect of the forebody compression surface. A further procedure is therefore needed by which the original Laval nozzle axis is shifted up (or rotated) by an angle α_0 (step 4) until α_s is close to zero.

The addition of a second nozzle (step 5) introduces a further set of parameters that may be used favorably for an optimization of the thrust vectoring. Because of the necessary rotation (or lifting of the exit) of the primary nozzle by the angle α_0, the lower nozzle lip (cowl) now will have a negative angle with the outer flow. Ideally, this would allow the outer flow to expand into this region, but in reality a flow separation will be induced at the ramp, increasing the system drag. A second nozzle can, among other effects, eliminate this drag. What seems to be more important is the improvement of the thrust vector control (size and angle) by creating a kind of gas dynamic wall for the lower edge of the primary jet, producing flow expansion into the outer flow and reducing flow separation at the cowl, thereby reducing overexpansion and flow separation at the ramp contour.

III. Basic Approach

We shall approach this complex multiparameter system by introducing a number of simplifications that will be discussed and justified in the following.

On the basis of the evaluation of slit jet properties, it should be possible to treat only the simpler two-dimensional problem. It is to be expected that results will be most realistic in the nozzle near field but less reliable in the far field where three-dimensional flow is expected to prevail. Furthermore, details of the actual nozzle width are currently not known. Apart from these practical reasons it is more important to try to understand the physical nature of the more simple two-dimensional flow in this exploratory study, before looking at the more complicated three-dimensional flow.

As a further simplification, boundary layers generated inside the nozzle and near the lower cowl are neglected, and perturbations of the outer flow by the hypersonic cruise vehicle forebody caused by oblique shock and rarefaction waves are ignored. As a result, the thrust vector $\boldsymbol{S}$ will be calculated with the reference pressure p_a assumed to exist at the foreward and upper control surface, and friction at the ramp will be neglected in this case. Although the following study will show that mixing layers can play a role and that there is a potential to influence the jet channels by the mixing layers, we shall not include a turbulence model for reasons of simplicity. However, at a later stage the inclusion of such a model will be a logical further step.

Starting from the full Navier–Stokes equations, we write the conservation equations in conservative form:

$$\frac{\partial}{\partial t}\boldsymbol{U} + \frac{\partial}{\partial x}\boldsymbol{F}(\boldsymbol{U}) + \frac{\partial}{\partial y}\boldsymbol{G}(\boldsymbol{U}) = 0 \tag{1}$$

with

$$\boldsymbol{U} = \begin{Bmatrix} \rho \\ \rho u \\ \rho v \\ \rho E \end{Bmatrix} \qquad \boldsymbol{F} = \begin{Bmatrix} \rho u \\ \rho u^2 + p - \tau_{xx} \\ \rho uv - \tau_{xy} \\ \rho uH - u\tau_{xx} - v\tau_{xy} + q_x \end{Bmatrix}$$

$$\boldsymbol{G} = \begin{Bmatrix} \rho v \\ \rho uv - \tau_{xy} \\ \rho v^2 + p - \tau_{yy} \\ \rho vH - v\tau_{yy} - u\tau_{xy} + q_y \end{Bmatrix}$$

The sum of internal and kinetic energy and the total enthalpy, respectively, are

$$E = \frac{p}{(\gamma - 1)\rho} + \frac{1}{2}(u^2 + v^2), \qquad H = E + \frac{p}{\rho}$$

Here, the molecular momentum and energy fluxes, respectively, are

$$\tau_{xx} = \tfrac{2}{3}\mu(2u_x - v_y), \qquad \tau_{xy} = \mu(u_y + v_x)$$

$$\tau_{yy} = \tfrac{2}{3}\mu(2v_y - u_x), \qquad q_x = -\lambda_t T_x, \qquad q_y = -\lambda_t T_y$$

The equation of state is $p = \rho R_g T$. The temperature dependence of the transport coefficients, the viscosity μ and the thermal conductivity λ_t, are approximated by a power law with the coefficient $\omega = 0.62$.

The system is nondimensionalized by using the length R_0 and state quantities of the outer flow:

$$\rho_a,\ p_a,\ T_a,\ c_0 = \sqrt{R_g T_a}$$

and nondimensionalized quantities will be marked by a tilde. A mapping of the physical plane $[x, y]$ onto a rectangular plane $[\xi, \eta]$ is performed by the transformation

$$\eta = y/R(x), \qquad \xi = x/L$$

To improve the resolution in the boundary layer and the nozzle near region, the grid is continuously clustered towards the ramp contour and the nozzle exits.

An explicit predictor-corrector scheme with a second-order Harten–Yee[11]-type total variation diminishing (TVD) scheme is used. Dissipative and diffusive terms are discretized by using central differencing. In the TVD scheme the following limiter function[11] is used:

$$\hat{Q}_{j+\frac{1}{2}} = \text{minmod}\left[2\Delta_{j-\frac{1}{2}},\ 2\Delta_{j+\frac{1}{2}},\ 2\Delta_{j+\frac{3}{2}},\ \tfrac{1}{2}\left(\Delta_{j-\frac{1}{2}} + \Delta_{j+\frac{3}{2}}\right)\right]$$

In the TVD scheme the entropy correction parameter is $\delta_e = 0.1$ and constant; cell interface values are calculated by Roe's approximate Riemann solver. The Courant–Friedrichs–Lewy condition is equal to 0.8, if the Reynolds number $Re_0 > 10^3$. Otherwise, an approximate cell Reynolds number[12] is calculated from $Re_\Delta = Re_0/j_{\max}$, where $j_{\max}$ is the number of grid points across the flowfield. From MacCormack's empirical formula for the time step, $\Delta t \le \Delta t_{\text{CFL}}/(1 + 2/Re_\Delta)$, the reduced time step is chosen.

For the upstream boundary conditions, the state in the nozzle exits is calculated from the stagnation states using isentropic relations, and outside the nozzles the outer flow state $\boldsymbol{W}_a$ is used. At the upper contour, the velocity $\boldsymbol{u}_w = 0$ and the wall is assumed to be adiabatic. At the downstream boundary, linear extrapolation is used in case of supersonic flow, and a method of characteristics for subsonic regions.[13]

Convergence and accuracy were tested using a single SERN nozzle. The number of grid points N_g was varied from $(51 \times 24) = 1224$ to $(201 \times 96) = 19{,}296$. A power law with an exponent $\kappa_{x,y}$ was used for the clustering. The residual $\Delta\rho = \sum_{i,j} |(\tilde{\rho}^{n+1} - \tilde{\rho}^n)|$ and the maximum $\Delta\rho_{i,j}$ were monitored during calculation. It was found that a relation $\Delta\rho \sim n^{-3.4}$ described the decrease of $\Delta\rho$ to a point where a final value of $\Delta\rho_{\text{cell}} \approx 1.45 \times 10^{-7}$/grid point was reached. For $N_g = 1224$, a steady state was reached at $n_\infty = 2500$. For larger N_g and for $\kappa_{x,y} > 1$, the exponent 3.4 decreases at later stages, and the transition to the steady state is delayed, increasing the number of steps n_∞ by a factor of 2–3. Variation of $\kappa_{x,y}$ from 1.0 to 1.6 also resulted in an increase of n_∞ by a factor of 5.5. The influence of N_g on the accuracy of the flowfield calculation was tested by observing the change of the thrust vector S and its angle α_s. Varying N_g from 1224 to 19,296 causes a change from $\alpha_s = 6.07$ deg to the asymptotic value $\alpha_s = 2.49$ deg. Further clustering causes small fluctuations given by $\alpha_s = 2.49 \pm 0.07$ deg. The value of S changes for the same variation from 9.76 to 11.27 N/cm and for the clustering study the variation is $S = 11.2 \pm 0.5$ N/cm. For most runs $N_g = (141 \times 71)$ was employed with $\kappa_x = 1.4$ and $\kappa_y = 1.2$.

IV. Design Case

Starting with the design case, the outer flow conditions are chosen as $p_a = 5$ mbar, $T_a = 200$ K, and $M_a = 6.0$. This yields the following pitot pressure and stagnation conditions: $p_{\text{pitot}} = 234$ mbar, $p_{a0} = 7.88$ bar, and $T_{a0} = 1639$ K. When we further select an ideal nozzle exit temperature of $T_{ne} = 275$ K and a cross section $R_0 = 0.25$ cm, the contour of an ideal Laval nozzle can be calculated. In our case we chose a contour that consists of three circular segments. The subsequent design procedure follows the previous description, where the inner flow in the nozzle is only of interest for determining the upstream boundary condition. For all following variations, the ramp contour $R(x)$ will have a constant radius of curvature of $R_3 = 193$ cm and a constant stagnation state of the primary nozzle, $\boldsymbol{W}_{10} = (3$ bar, 1714 K).

A. Preliminary Tests

We begin with a case of equal stagnation conditions, $\boldsymbol{W}_{20} = \boldsymbol{W}_{10}$, and a small fraction of the mass flux $\dot{m}_1$ of the primary nozzle, $\dot{m}_2 = C_b \dot{m}_1$, will be expanded in the secondary nozzle to ambient conditions, $p_{2e} = p_a$, whereas the upper and lower exit angles of the primary nozzle, $\beta_{1u} = \text{arctg}(\text{d}R/\text{d}x)_e$ and $\beta_{1l} = \alpha_0$, respectively, will be kept constant. We shall try to vary the lower angle of the secondary nozzle, β_{2l}, for some cases, but we assign $\beta_{2u} = \alpha_0$ and $\beta_{2l} = 0$. The iso-Mach and isobar fields of Fig. 2 indicate that the jet issued from the second nozzle overexpands, thereby helping the primary jet to expand into the lower region and to overexpand along the contour. This results in an onset of flow separation at the end of the ramp, since the wall pressure is $\tilde{p}_w < 1$ at $x \ge 14$ cm. Note that for this type of nozzle the outer flow is not deflected by a plume shock but rather expanded shock free into this low-pressure plume region (this holds only for the near field).

The change of the lower nozzle lip angle from zero to $\beta_{2l} = \alpha_0$ reduces the overexpansion of the secondary jet but has little influence upon the primary jet channel, Fig. 3. Now $\tilde{p}_w < 1$ at $x > 13.8$ cm.

Apparently, the possibilities to influence the state in the primary jet channel by a high enthalpy secondary jet are rather limited. This

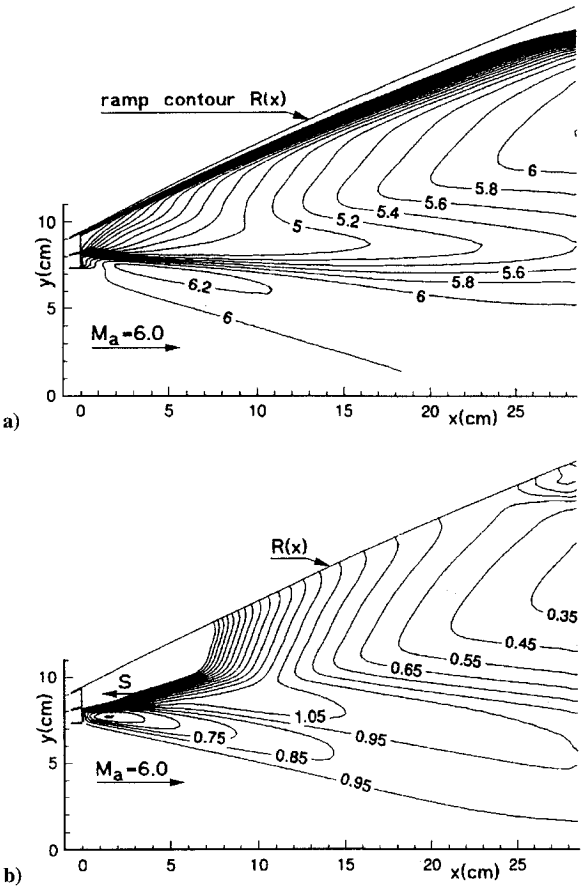

Fig. 2 Design case: a) iso-Mach lines and b) isobar lines. Stagnation states: W_{20} = W_{10} = (3 bar, 1714 K). Outer flow: p_a = 5 mbar, T_a = 200 K, and M_a = 6.0. Second nozzle mass fraction C_b = 0.15, exit Mach number M_{1e} = 3.0, and exit pressure $p_{2e} = p_a$. R_0 = 0.25 cm, Re_0 = 516, α_0 = 16 deg, and β_{2l} = 0 deg. Thrust S = 12.8 N/cm.

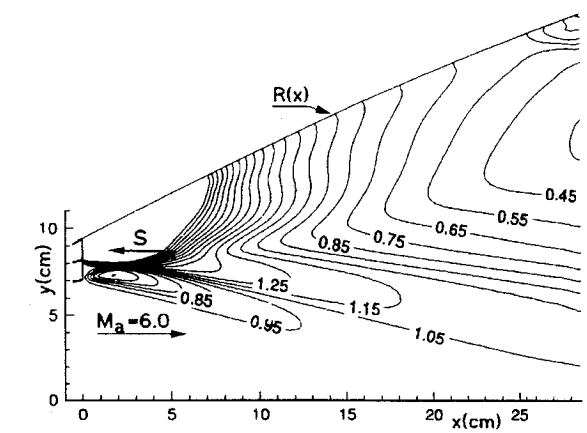

Isobar lines p/p_a

Fig. 3 Isobars for design case. Same data as in Fig. 2, except $\beta_{2l} = \alpha_0$.

leads us to explore the effects of a cold secondary jet. We choose a state with W_{20} = (1 bar, 100 K) and C_b = 0.5; see Fig. 4. The primary jet channel is narrower now, and consequently the expansion is slower. The pressure along the secondary jet channel balances the primary jet pressure, and a strong plume shock appears because of the strong shearing interaction that prevents the secondary jet from turning downwards. Because of the shear on both sides of the secondary jet and the pressure fanned down from the primary jet, pressure builds up over a distance of about 2 cm downstream of the nozzle exit and reduces the Mach number from M_{2e} = 4.2 at the exit to 1.4 at maximum channel pressure. Beyond this point, the pressure is decreasing very slowly (less than in the primary jet channel),

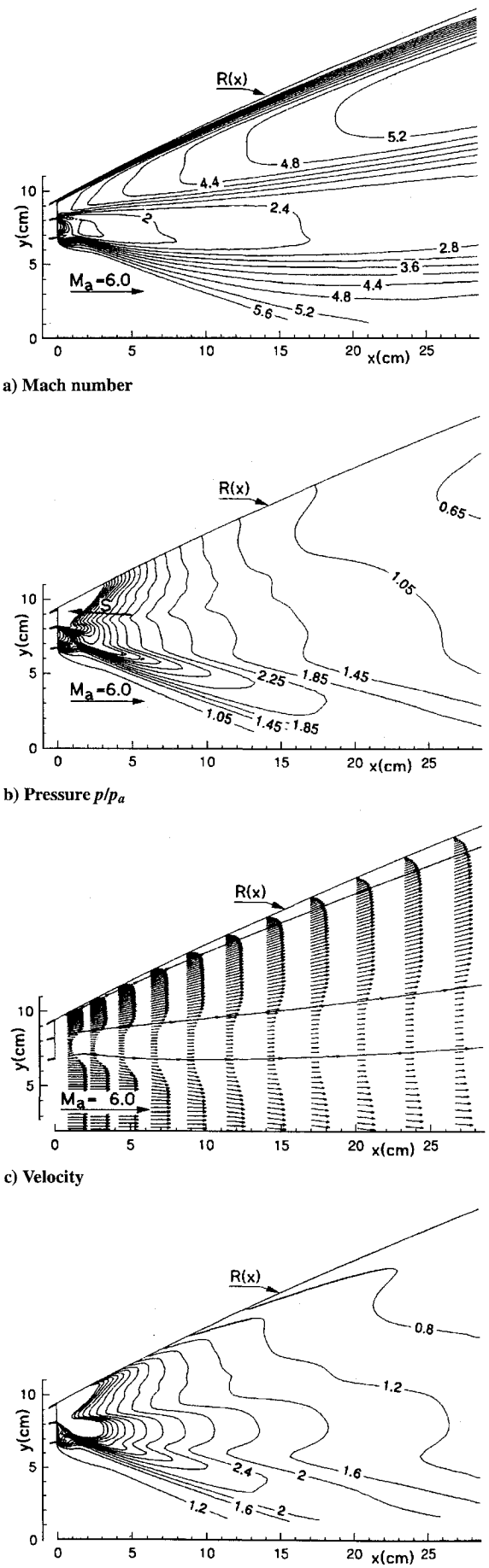

Fig. 4 Design case with same data as in Fig. 2, except W_{20} = (1 bar, 100 K), $\beta_{2l} = \alpha_0$, and C_b = 0.5.

and the flow is slightly accelerated. The velocity field is depicted in Fig. 4c, where the growth of the mixing layer can be observed. One may ask why the gas wall properties are superior for a cold secondary jet when compared with a high enthalpy jet. From the plot of the lines of constant impedance, ρc, one may conclude that pressure perturbations originating in the primary jet channel will be reflected at the harder wall of the cold jet having a larger impedance.

B. Secondary Nozzle Exit Pressure Variation

After these exploratory tests it seems feasible to look more systematically at the sensitivity and performance of the system with respect to certain parameters. Keeping the state W_{10} at the values given in Fig. 4 and with a constant mass flux fraction $C_b = 0.5$, we start with a variation of the secondary nozzle exit pressure p_{2e}. The range will be limited to $p_a \leq p_{2e} \leq p_{1e}$, since a pressure larger than that at the primary nozzle exit will lead to its choking and strong shock reflections. This does not necessarily result in a poorer performance, but it will be a much more complicated problem. Increasing p_{2e} is achieved by cutting the nozzle. This also results in a decrease of the exit cross section from $D_2 = 1.18$ cm for $\tilde{p}_{2e} = 1$ to $D_2 = 0.19$ cm for $\tilde{p}_{2e} = 16.8$ and in a decrease of the exit Mach number from $M_{2e} = 4.21$ to 2.27. For a single nozzle, this would reduce the efficiency, but for the twin nozzle this is not necessarily the case as can be seen in Table 1, where the value of the thrust vector and the wall pressure at some typical positions are given for a set of different values for p_{2e}. Apparently there exists an optimum for $\tilde{p}_{2e} \approx 4$ where the recompression in the secondary jet channel near the nozzle exit caused by the expansion fan from the primary nozzle and the action of the shear layers disappears. In Fig. 5 the iso-Mach and the isobar fields near the nozzle exit are shown for $\tilde{p}_{2e} = 4$. A decrease of the secondary jet Mach number still remains near the nozzle exit followed by a very slight increase further downstream.

C. Secondary Nozzle Mass Flux Variation

Because of the increase in pressure p_{2e}, the exit cross section of the secondary nozzle is reduced. The size of the secondary jet plume also shrinks, which will diminish its influence upon the primary jet channel. Another variation is therefore attempted. The mass flux of the secondary nozzle, $\dot{m}_2 = C_b \dot{m}_1$, is changed, while $\tilde{p}_{2e} = 6$ is kept constant.

When increasing C_b, the thrust also grows, which in part is caused by the larger overall mass flux and in part is caused by the larger wall pressure p_w at the ramp. One may separate the influence of the increased mass flux by introducing a reference thrust

$$S_{\text{ref}} = \frac{1}{1 + C_b u_{2e}/u_{1e}} S \tag{2}$$

The slight increase of S_{ref} with C_b (see Table 2) is in accordance with a growth of the wall pressure.

Table 1 Secondary nozzle exit pressure variation

p_{2e}	S, N/cm	α_s, deg	$\tilde{p}_{w1}$	$\tilde{p}_{w2}$	$\tilde{p}_{w3}$	$\tilde{p}_{w4}$
2	13.9	4.59	2.52	1.56	1.11	0.86
4	15.0	5.76	2.96	1.82	1.28	0.98
6	13.9	5.87	2.84	1.43	0.99	0.76
8	14.0	6.35	2.39	1.37	0.94	0.72
16.9	13.8	6.69	2.30	1.32	0.89	0.69

Table 2 Mass flux variation

C_b	S, N/cm	S_{ref}, N/cm	α_s, deg	$\tilde{p}_{w1}$	$\tilde{p}_{w2}$	$\tilde{p}_{w3}$	$\tilde{p}_{w4}$
0.2	13.0	12.4	5.09	2.22	1.24	0.82	0.62
0.5	13.9	12.6	5.86	2.48	1.43	0.99	0.76
1.0	15.9	13.1	6.52	3.26	1.99	1.38	1.05
1.5	17.4	13.2	6.41	3.61	2.33	1.63	1.24
2.0	19.0	13.3	6.22	3.75	2.67	1.90	1.45

Table 3 Influence of stagnation temperature

T_{20}, K	S, N/cm	α_s, deg	$\tilde{p}_{w1}$	$\tilde{p}_{w2}$	$\tilde{p}_{w3}$	$\tilde{p}_{w4}$
200	15.9	4.00	2.70	1.80	1.31	1.02
500	15.7	2.73	2.31	1.58	1.18	0.93
1000	15.7	2.28	2.11	1.49	1.15	0.90

Table 4 Primary nozzle exit Mach number variation

M_{1e},	S, N/cm	α_s, deg	$\tilde{p}_{w1}$	$\tilde{p}_{w2}$	$\tilde{p}_{w3}$	$\tilde{p}_{w4}$
2.0	13.2	8.24	1.29	0.80	0.56	0.65
2.5	14.3	5.74	1.82	1.15	0.81	0.64
3.0	15.9	4.00	2.70	1.80	1.31	1.02

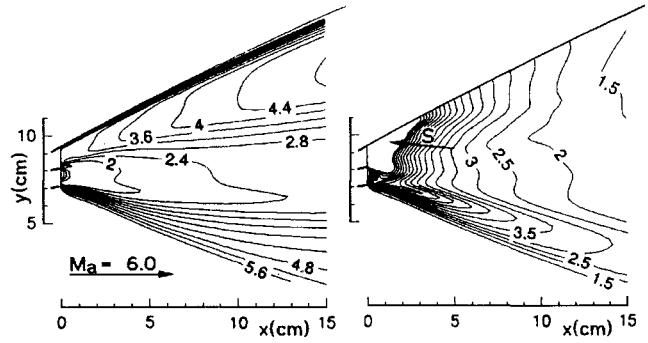

a) Mach number b) Pressure p/p_a

Fig. 5 Design case with same data as in Fig. 2, except $p_{2e} = 4p_a$ and $C_b = 1.0$.

D. Secondary Nozzle Stagnation Temperature

For ideal isentropic flow conditions in a nozzle, the thrust is not altered when increasing the stagnation temperature T_{20}. But the mass flux is reduced for a constant thrust. We shall keep $\tilde{p}_{2e} = 4$ and $D_2 = D_1$, i.e., the secondary nozzle contour will be constant. As might be expected from the previous results, the wall pressure p_w decreases when T_{20} grows, and the thrust S remains practically constant. However, the thrust vector angle shifts from $\alpha_s = 4.02$ to 2.28 deg because of the wall pressure reduction; see Table 3.

E. Primary Nozzle Exit Mach Number

Originally, there exists a certain arbitrariness when designing the primary nozzle. From the design point of view, it would be advantageous to set the Mach number M_{1e} as small as possible. However, this would increase the expansion of the jet plume into the lower field and cause an overexpansion at the ramp at an early stage. As indicated in Table 4, not only the thrust vector decreases with a reduction of M_{1e} (achieved by cutting the primary nozzle), but also p_w is reduced. The thrust vector angle α_s grows by a factor of 2.

V. Off-Design Case

When the pressure ratio Π is reduced for a given ramp contour, overexpansion in the primary jet channel will increase the drag of the system and cause a dramatic rotation of the thrust vector to negative angles of $\alpha_s = -20$ deg. Smaller angles will occur, if recompression at the ramp is induced and stabilized. In general, shock recompression will occur under the influence of three-dimensional flow effects.[1] It has been shown in the previous sections that the twin nozzle is able to delay flow separation and can improve thrust vector control. In the following, the performance of the system will be studied when Π is reduced. A few examples of wall bleeding will also be discussed for very small pressure ratios ($\Pi \leq 15$).

A. Variation of the Pressure Ratio Π

In any practical application the variation of Π will be accompanied by changes of the Mach number M_a, overall thrust S, mass fluxes $\dot{m}_i$, stagnation conditions W_{i0}, and nozzle exit Mach number M_{1e}. Since actual flight conditions are difficult to estimate at

Table 5 Parameters for Π variation

Π	M_a	p_{pitot}, bar	ϵ^*	M_{1e}	p_{20}, bar
600	6.00	0.23	1.00	3.00	1.00
300	5.13	0.34	1.55	2.52	1.35
150	4.38	0.50	2.17	2.15	1.65
60	3.54	0.83	3.05	1.73	1.70
30	3.00	1.21	3.60	1.47	2.00
15	3.00	2.41	3.60	1.47	2.00

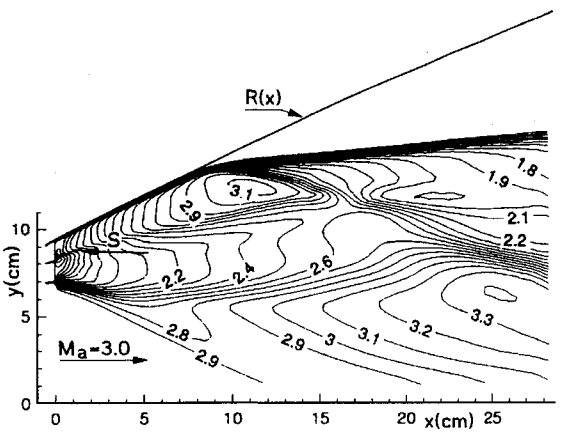

a) Mach number

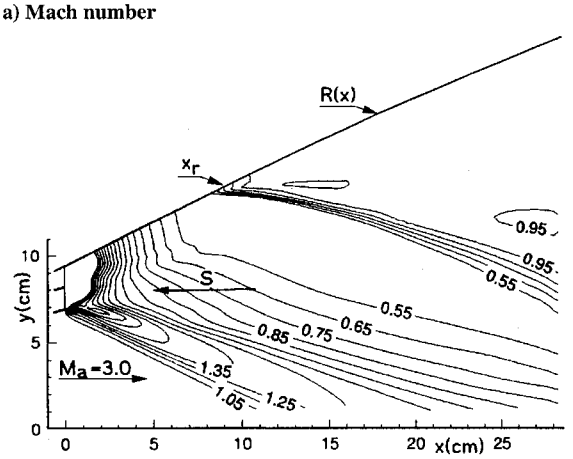

b) Pressure p/p_a

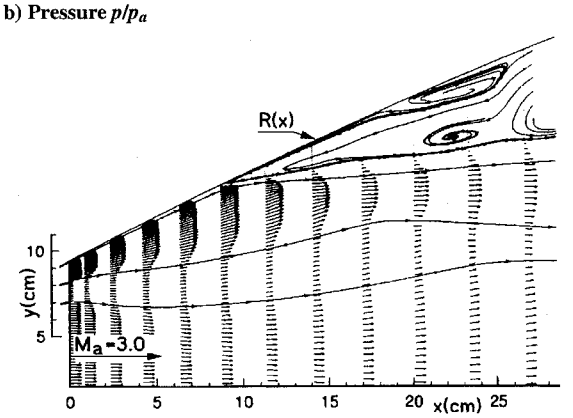

c) Velocity

Fig. 6 Off-design case with pressure ratio Π = 15. Data different from those in Fig. 2: W_{20} = (2 bar, 200 K); p_a = 0.2 bar, T_a = 200 K, M_a = 3.0; C_b = 2.2, M_{1e} = 1.5, $p_{2e} = 4p_a$; ϵ^* = 3.6, $Re_0 = 2 \times 10^4$, and S = 64.7 N/cm.

present, simple plausible variations for these parameters are introduced. These changes apply only to the most pertinent parameters not to mix different counteracting effects. The increase of the drag force with Π can only in part be covered by augmenting the thrust vector S (or rather the mass fluxes). Therefore, in addition the cruise speed or M_a has to be reduced. The set of parameters that has been used in the present calculations is given in Table 5.

Table 6 Variation of flight conditions

Π	S, N/cm	S_{red}, N/cm	α_s, deg	x_r, cm	$\tilde{p}_{w1}$	$\tilde{p}_{w2}$	$\tilde{p}_{w3}$	$\tilde{p}_{w4}$
600	15.9	15.9	4.00	28.0	2.70	1.80	1.31	1.02
300	24.7	15.9	4.37	28.0	2.15	1.40	0.99	0.77
150	35.1	16.2	3.84	27.0	1.65	1.03	0.72	0.55
60	48.8	16.0	1.05	24.4	1.02	0.62	0.43	0.38
30	59.9	16.6	−0.16	17.6	0.68	0.41	0.56	0.94
15	64.7	18.0	−0.54	9.0	0.53	1.01	1.02	1.01

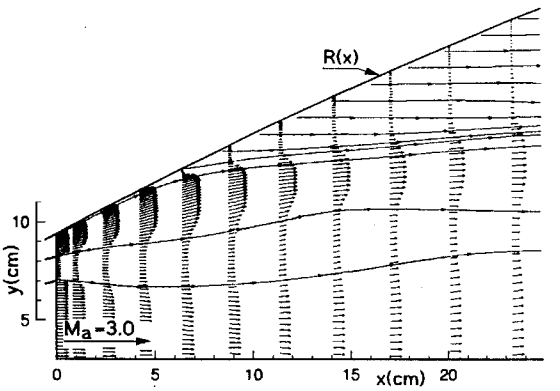

Fig. 7 Pressure ratio Π = 15. Gas injection (full bleeding) at the ramp, until $p_w \geq p_a$. All other data same as in Fig. 6.

The pitot pressure is included in Table 5, since it provides some measure of the tolerable flight speed. All other parameters have values as given in Fig. 6 and are kept constant. Note that, for a constant ramp contour, an increase of the throat cross section by the factor ϵ^* is equivalent to a rescaling of the Laval reference nozzle. This is a favorable step, since it reduces overexpansion. But this rescaling is still not sufficient to avoid overexpansion for small Π. The reduction of M_a also requests some reduction of M_{1e}, and p_{10} has to be increased to maintain supersonic conditions in the secondary jet channel.

When changing Π from 300 to 30 (see Table 6), the reduced thrust vector $S_{\text{red}} = S/\epsilon^*$ remains almost constant, α_s changes slightly from +4 to −1 deg, and the shock recompression point x_r moves upstream along the ramp, when Π < 50.

B. Wall Bleeding

The fields of Mach number, pressure, and velocity in Fig. 6 indicate that a rather complex structure exists for a pressure ratio of Π = 15. When the back pressure p_a creeps upstream inside the boundary layer of the ramp, this results in the buildup of an oblique slightly curved shock wave with a recompression zone at x_r = 9 cm and flow separation. The primary and secondary jet channels, their deflection by the shock wave, and the recompression can be observed in the iso-Mach field and the velocity field. The downstream boundary condition allows for a recirculating flow, and we assume a flow condition changing isentropically from a stagnation state W_a with $u_a = 0$. Without knowing the complete shape of the hypersonic cruise vehicle and without extension of the computational domain to the full region around the vehicle including all perturbed flow regions, there remains some arbitrariness in selecting boundary conditions for subsonic regions.

For situations where the real three-dimensional flow may not allow to adjust in such a way that the jets find boundary conditions corresponding to those given earlier, one can still influence the (near) nozzle jet field by bleeding. One first step toward this way of control is shown in Fig. 7, where the velocity field is plotted for a case with subsonic wall bleeding (u_w = positive, $v_w = 0$), until locally the pressure $\tilde{p}_w \geq 1$. There exists a shear layer between the jet channels and an upper gas cushion where the pressure is practically constant and equal to 1, similar to that in Fig. 6, but the shock wave has disappeared completely. The jet channel cross sections change smoothly, and the thrust vector control is satisfactory. In Fig. 8, the distributions of the wall pressure p_w and the

Table 7 Sectional bleeding

Case no.	$\tilde{v}_w$	S, N/cm	α_s, deg	x_r, cm	x_{min}, cm	x_{max}, cm	$\tilde{p}_{w1}$	$\tilde{p}_{w2}$	$\tilde{p}_{w3}$	$\tilde{p}_{w4}$
1	−0.50	73.2	11.80	5.5	9.4	11.6	1.61	1.48	1.27	1.21
2	−0.25	68.0	5.03	6.2	7.3	9.4	1.00	1.13	1.12	1.06
3	−0.25	67.0	3.35	4.6	5.4	7.3	0.98	1.04	1.02	0.98
4	−0.50	66.1	1.74	4.3	5.4	7.3	0.90	0.91	0.93	0.96
5	−0.75	69.8	7.35	3.8	5.4	7.3	1.09	1.11	1.08	1.05
6	−0.50	64.9	−0.22	8.0	9.4	9.6	0.94	0.99	0.99	0.98

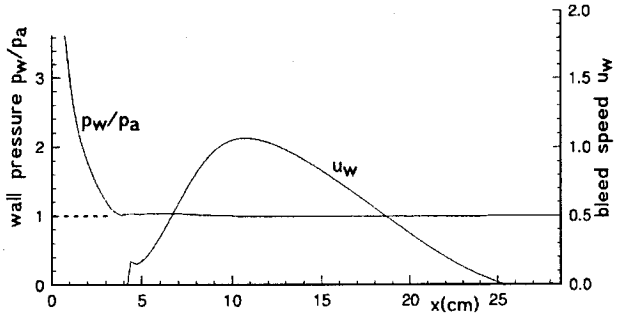

Fig. 8 Wall pressure p_w and gas injection speed $\tilde{u}_w$ at the ramp contour $R(x)$ as function of x; conditions as in Fig. 7.

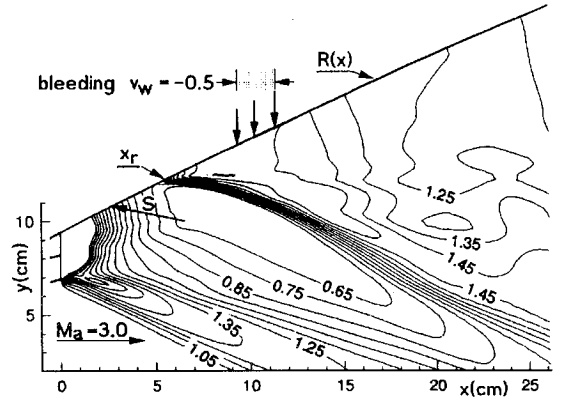

a) Pressure p/p_a

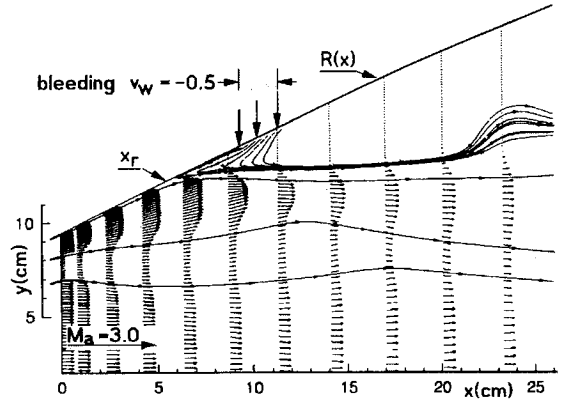

b) Velocity

Fig. 9 Pressure ratio Π = 15. Sectional gas injection, downstream of the natural recompression point x_r, at x = 9.4–11.6 cm with $\tilde{v}_w = -0.5$. Same data as in Fig. 6.

bleed speed u_w, respectively, are plotted as function of x. The thrust vector control is satisfactory; however, the cost of this method is inacceptably high. The mass flux needed for this procedure comprises a considerable fraction of the primary nozzle flux, $\dot{m}_{bleed} = 0.35\dot{m}_1$. This makes it difficult to apply this method in a practical design, even if only low enthalpy gas could be used and three-dimensional effects might reduce the surface available for full bleeding.

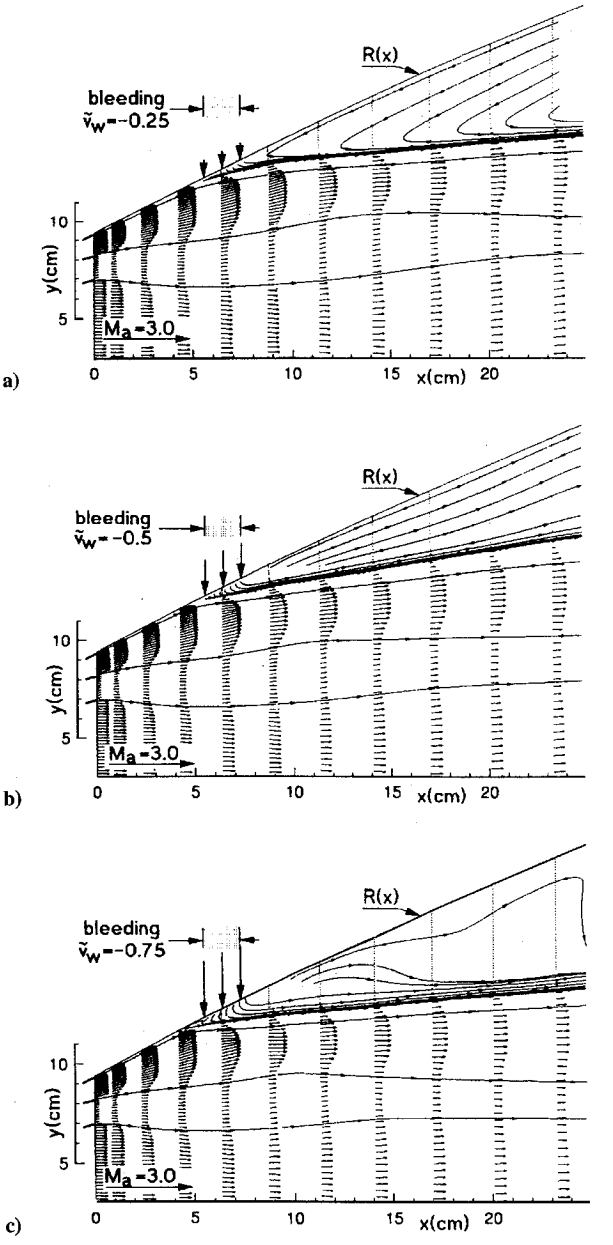

Fig. 10 Velocity fields for sectional gas injection at x = 5.4–7.3 cm. Variation of bleeding gas speed: $\tilde{v}_w = -0.25$, -0.5, and -0.75. Same data as in Fig. 6.

Probably a more elegant and less expensive way to control the thrust vector for off-design situations is by partial or sectional bleeding. Here, we take advantage of the neutralizing effect of the recompression shock with respect to the force balance at the ramp and try to stabilize and manipulate the shock position by bleeding in small sections of the ramp. It turns out that this is most efficiently achieved by blowing into negative y direction, i.e., $\boldsymbol{u}_w = (0, v_w)$ with $\tilde{v}_w < 0$.

We begin for case 1 (see Table 7) with a sectional bleeding at x = 9.4 − 11.6 cm, a region that is downstream of the natural recompression zone at x_r = 9 cm; see Fig. 6. As might be expected, this perturbation of the supersonic flow in the primary jet channel creates a shock layer by itself that then merges with the natural shock system; see Fig. 9. As a result of this bleeding, a considerable displacement of the shock upstream, with x_r = 5.5 cm, is achieved. The wall pressure at the ramp is increased considerably, resulting in an augmentation of S by 13% and a rotation of the vector towards positive angles by 11.3 deg.

Moving the bleeding section further upstream seems to be less efficient; see case 2. The increase of v_w, cases 3–5, moves x_r upstream and has an influence on the thrust vector angle α_s. The pressure fields in Fig. 10 and the velocity fields in Fig. 11 show the changes that

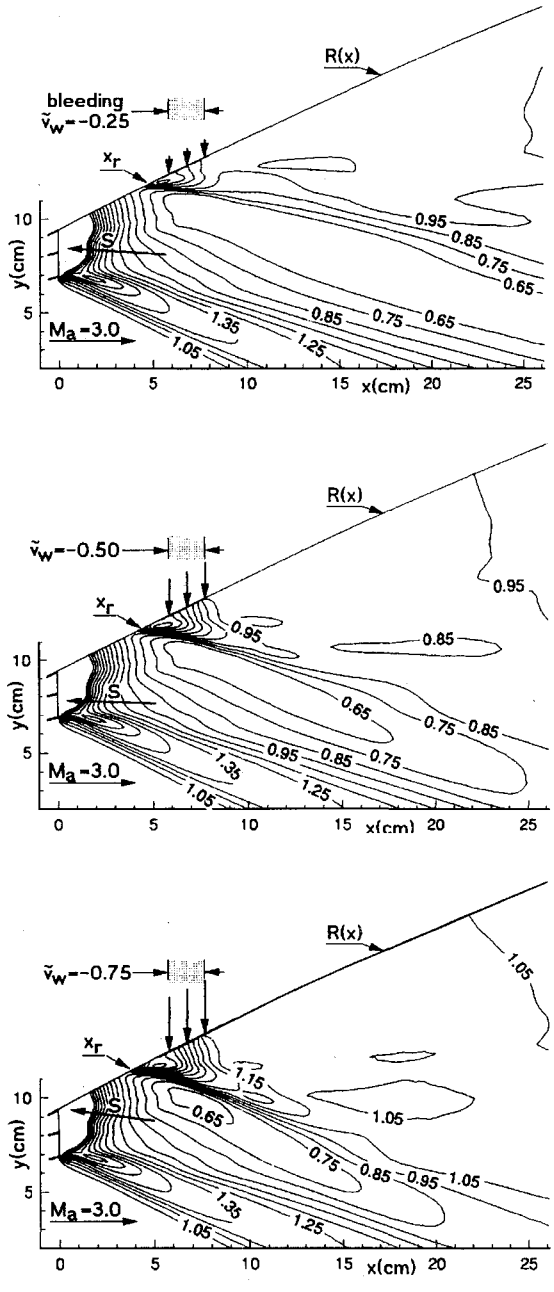

Fig. 11 Pressure fields (p/p_a) for the same cases as shown in Fig. 10.

are induced when v_w is increased. Even bleeding from a narrow slit with $\tilde{v}_w = -0.5$, case 6, has a stabilizing effect.

Keep in mind that these examples of sectional bleeding treat the extreme case of $\Pi = 15$. It can be expected that for any less dramatic set of parameters the application of small amounts of sectional bleeding at some points distributed along the ramp contour will provide an efficient means to control the thrust vector.

VI. Concluding Remarks

Previous investigations of SERN models and systems with bypass nozzles have lead to the conclusion that there is a need for studying more systematically the off-design behavior of such propulsion systems. To keep the degree of complexity low, a planar twin-nozzle system was studied with respect to a number of parameter variations. Exploratory studies of the design case indicated that most efficient control through the secondary nozzle is achieved when the stagnation temperature of its flow is low. Apparently the secondary jet channel acts like a gasdynamic wall because of its locally higher acoustic impedance. To apply this effect to a favorable thrust vector control, size and shape of the secondary jet channel are to be formed by a proper choice of the nozzle parameters and the mass flux. However, for far off-design situations, for a pressure ratio of 10 or less, neither the secondary nozzle nor the rescaling because of larger primary mass fluxes can prevent the primary jet from overexpansion, recompression by shock waves, and flow separation. In this case subsonic gas injection at certain sections of the ramp contour can favorably influence and stabilize the flowfield.

To a certain extent, the interaction between the different jet channels leads to problems of confined compressible mixing that will require further studies, including turbulence. The influence is expected to be strong in the near field that has the strongest effect upon the shaping of the total jet plume. Therefore, it seems sensible to investigate the planar problem first, before looking at the three-dimensional structure of the flow around the complete hypersonic cruise vehicle contour.

Acknowledgment

This work is related to Project C6 of Sonderforschungsbereich 253, which was in part financially supported by the Deutsche Forschungs-Gemeinschaft.

References

[1]Zeutzius, M., and Beylich, A. E., "Experimental Investigation of Asymmetric Nozzles for Advanced Hypersonic Space Planes—Structure of Nozzle Jets and Thrust Vector Control," *Zeitschrift für Flugwissenschaften und Weltraumforschung*, Vol. 17, No. 5, 1993, pp. 311–322.

[2]Zeutzius, M., "Überschalldüsen für Hyperschallfluggeräte mit Schubvektorsteuerung," Dissertation, Mechanical Engineering, Technische Hochschule Aachen, Germany, 1994.

[3]Beylich, A. E., and Zeutzius, M., "Performance and Control of Asymmetric Nozzle Jets," *Proceedings of the Asian-Pacific Conference on Aerospace Technology and Science*, International Academic Publishers, Beijing, PRC, 1994, pp. 917–922.

[4]Papamoschou, D., "Thrust Loss Due to Supersonic Mixing," *Journal of Propulsion and Power*, Vol. 10, No. 6, 1994, pp. 804–809.

[5]Ruffin, S. M., Venkatapathy, E., Keener, E. R., and Spaid, F. W., "Hypersonic Single Expansion Ramp Nozzle Simulations," *Journal of Spacecraft and Rockets*, Vol. 29, No. 6, 1992, pp. 749–755.

[6]Watanabe, S., "Scramjet Nozzle Experiment with Hypersonic External Flow," *Journal of Propulsion and Power*, Vol. 9, No. 4, 1993, pp. 521–528.

[7]Mitani, T., Ueda, S., Tani, K., Sato, S., Miyajima, H., Matsumoto, M., and Yasu, S., "Validation Studies of Scramjet Nozzle Performance," *Journal of Power and Propulsion*, Vol. 9, No. 5, 1993, pp. 725–730.

[8]Ishiguro, T., Takaki, R., Mitani, T., and Hiraiwa, T., "Three-Dimensional Analysis of Scramjet Nozzle Flows," *Journal of Propulsion and Power*, Vol. 10, No. 4, 1994, pp. 540–545.

[9]Berens, T., "Numerical Investigation of Thrust Vectoring by Injection of Secondary Air into Nozzle Flows," *AGARD Conference Proceedings 534, Computational and Experimental Assessment of Jets in Cross Flow*, 1993, pp. 11.1–15.

[10]Beylich, A. E., "Struktur von Überschallfreistrahlen aus Schlitzblenden," *Zeitschrift für Flugwissenschaften und Weltraumforschung*, Vol. 3, No. 1, 1979, pp. 48–58.

[11]Yee, H. C., "A Class of High Resolution Explicit and Implicit Shock Capturing Methods," NASA TM-101088, Feb. 1989.

[12]Anderson, D. A., Tannehill, J. C., and Pletcher, R. H., *Computational Fluid Mechanics and Heat Transfer*, Hemisphere, New York, 1984, Chap. 9.

[13]Cline, M. C., "VNAP: A Computer Program for Computation of Two-Dimensional, Time-Dependent Compressible, Viscous, Internal Flow," Los Alamos Scientific Lab., LA-7326, Los Alamos, NM, Nov. 1978.